Journal of Structural Geology, Vol. 15, No. 9/10, pp. 1061 to 1075, 1993
Printed in Great Britain

0191-8141/93 $06.00+0.00

Experimental deformation of muscovite

V. M. MARES* and A.K. KRONENBERG†

Center for Tectonophysics, Texas A&M University, College Station, TX 77843-3113, U.S.A.

(*Received* 23 *June* 1992; *accepted in revised form* 22 *December* 1992)

Abstract—The strength and mechanical anisotropy of muscovite have been investigated by shortening single crystals at 45°, 0° and 90° to the basal plane (001) at temperatures T from 20 to 400°C, confining pressures P_c from 10 to 400 MPa, and strain rates $\dot{\varepsilon}$ from 2.5×10^{-7} to 2.3×10^{-4} s^{-1}. Samples deformed as 45° to (001) exhibit smooth undulatory extinction in thin section associated with dislocation glide, with few well developed low-angle kink boundaries. Basal shear strengths depend on confining pressure at $P_c < 50$ MPa with a coefficient of internal friction μ of ~0.4, while shear strengths measured at 100–400 MPa appear to be insensitive to confining pressure. Results for samples shortened at $P_c \geq 100$ MPa at 45° to (001) and directions [001], [110], [310] and [010] within the basal plane suggest only a weak mechanical anisotropy within (001), corresponding to Burgers vectors ⟨100⟩, 1/2⟨110⟩ and 1/2⟨1$\bar{1}$0⟩. The effects of temperature and strain rate on glide strengths are relatively small. Assuming an exponential relationship between differential stress σ and strain rate $\dot{\varepsilon}$ of the form $\dot{\varepsilon} = A \exp(\alpha\sigma) \exp(-Q/RT)$, results from temperature- and strain rate-stepping experiments performed at $P_c = 200$ MPa yield an activation energy Q of 47 ± 19 kJ mol^{-1} and an exponential constant α of 0.5 ± 0.2 MPa^{-1}. Samples loaded parallel to the basal plane shorten by the development of sharply defined kink bands. Strengths associated with kink band formation are higher than those associated with glide in samples compressed at 45° to (001) and exhibit significant pressure dependence ($\mu \cong 0.8$) up to confining pressures of 200 MPa. Kink bands are generated at the ends of samples where contact is made with the pistons. Samples loaded at 90° to (001) are much stronger than samples of all other orientations and deformation is accomplished by fracture. Fracture strengths exhibit a strong dependence on confining pressure ($\mu \cong 0.9$), similar in magnitude to other silicates that are brittle at the same conditions. By comparison with biotite, muscovite is weaker in shear on (001) at the experimental conditions tested with an activation energy for glide, Q, that is significantly smaller than that for glide in biotite.

INTRODUCTION

EXPERIMENTAL studies of mica-bearing rocks such as slates, phyllites, schists and gneisses (e.g. Donath 1961, 1964, 1968, Paterson & Weiss 1962, 1966, Borg & Handin 1966, Gottschalk *et al.* 1990, Shea & Kronenberg 1992, 1993) have provided essential data on the strength and mechanical behavior of polymineralic mica aggregates. Micas are weak by comparison with other silicates that are common to rocks of the continental crust (e.g. quartz and feldspar, Carter *et al.* 1964, Christie *et al.* 1964, Borg & Heard 1970, Tullis & Tullis 1972, Marshall & McLaren 1977, Willaime *et al.* 1979, Tullis 1983, Koch *et al.* 1989) and have been shown to control the strengths and anisotropies of foliated rocks. However, data describing the inelastic single-crystal mechanical properties and deformation mechanisms of micas are limited to biotite (Etheridge *et al.* 1973, Kronenberg *et al.* 1990) and a single experiment performed on muscovite (Chester 1985).

Muscovite is dioctahedral with two of three octahedral sites occupied by Al, leaving one of every three sites vacant, and its mechanical properties may differ from those of biotite which is trioctahedral with all three octahedral sites occupied by Mg and Fe. The regular arrangement of occupied and vacant octahedral sites in muscovite results in distortions of the tetrahedral silicate layers as well as variations of the K–O bond lengths (Radoslovich 1960, Appelo 1979). Slip is thought to occur within the weakly-bonded interlayer regions (Baños *et al.* 1983) and dislocation mobility and overall mechanical strength of muscovite may be influenced by variations in K–O bonding, as well as nearby elastic distortions of octahedral layers. Transmission electron microscopy (TEM) of mica foils during shear (Meike 1989) suggests that Peierls valleys associated with tetrahedral layer distortions in muscovite are larger than those in biotite and result in preferred dislocation orientations with long screw dislocations oriented along ⟨100⟩, 1/2⟨110⟩ and 1/2⟨1$\bar{1}$0⟩, unlike the wavy dislocations of mixed character in biotite.

In this paper, we report the results of experiments designed to measure the basal shear strength of muscovite as a function of confining pressure, temperature, strain rate and shear direction. In addition, we report the strengths of muscovite compressed parallel and perpendicular to (001).

EXPERIMENTAL METHODS

Starting material

The single crystal of muscovite chosen for this study comes from Methuen Township, Ontario, Canada. This crystal is 50 mm in dimension measured perpendicular to cleavage, and 45 mm by 90 mm measured along the cleavage surfaces. It is clear, with a slightly greenish hue, silver in reflection, and has flat, undeformed cleavage

*Also at Department of Geology. Current address: Department of Geology, James Cook University of Northern Queensland, Townsville, Queensland 4811, Australia.
†Also at Department of Geophysics.

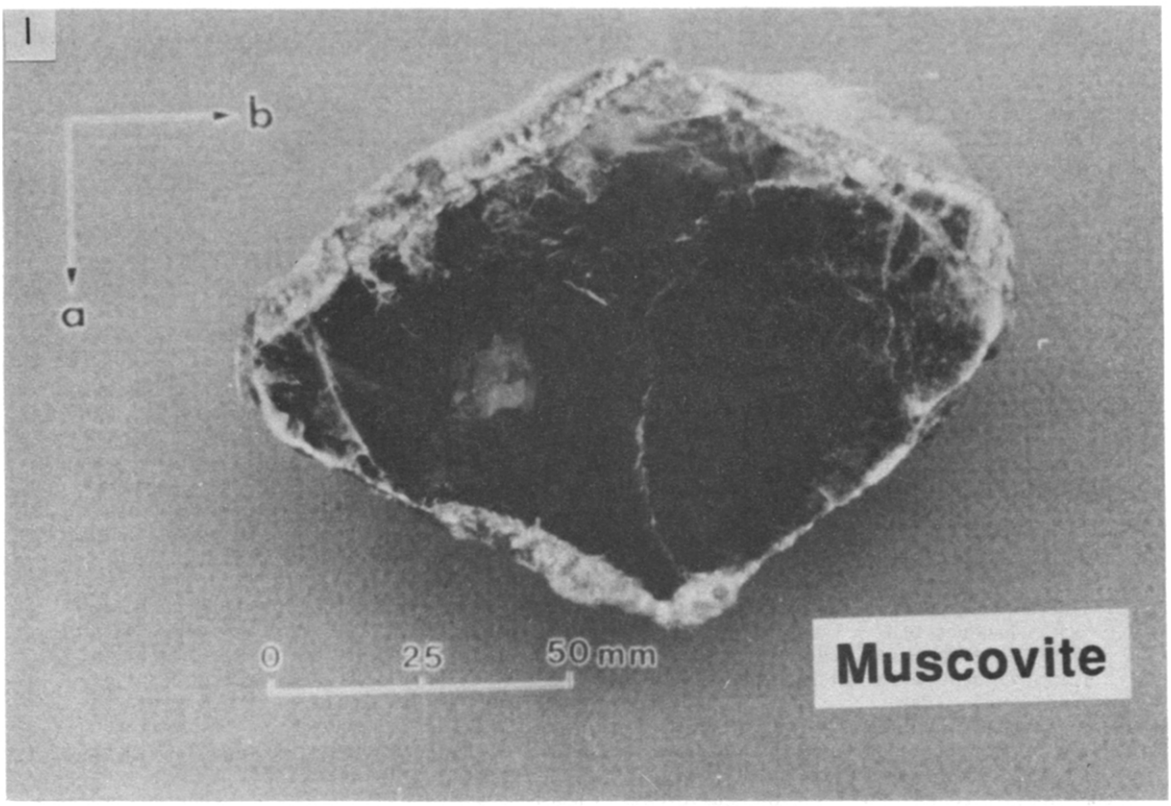

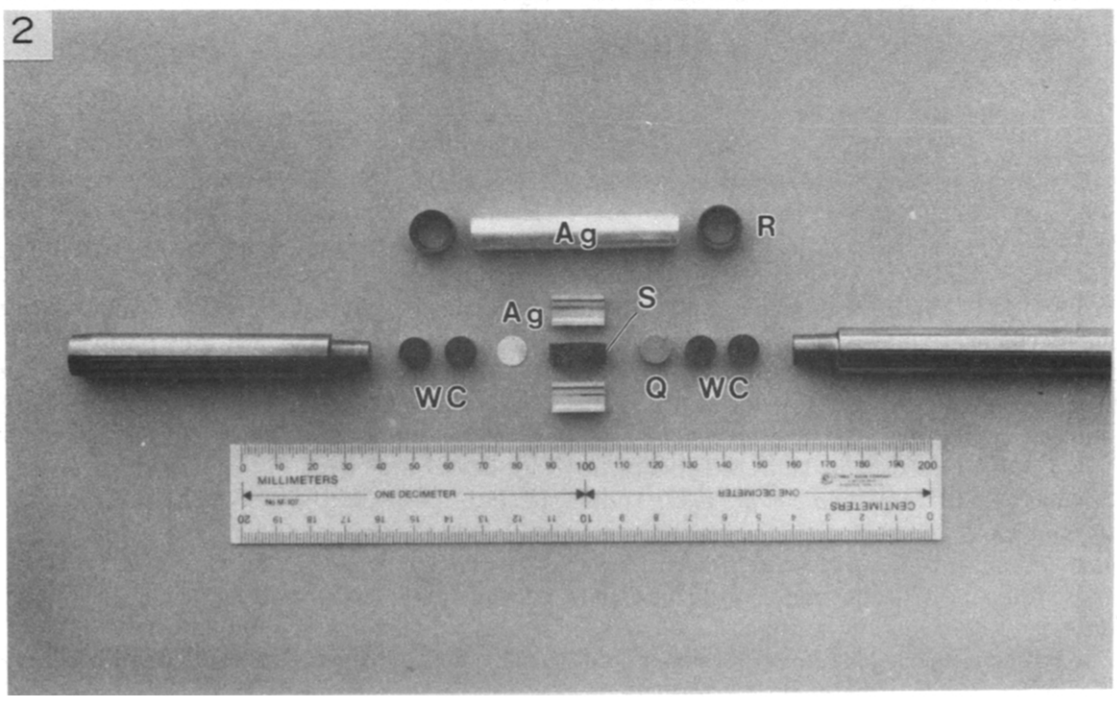

Fig. 1. Muscovite single crystal used as the starting material. The *a* crystallographic axis is oriented along the short diagonal and the *b* crystallographic axis along the long diagonal of the cleavage face.

Fig. 2. Sample assembly, showing sample (S), silver jackets (Ag), tungsten carbide (WC) and quartzite (Q) spacers, tungsten carbide pistons and sealing rings (R).

faces. The crystal displays {110} growth faces with the *a*-axis oriented along the short diagonal of its polygonal cleavage surfaces and the *b*-axis oriented along the long diagonal (Fig. 1). Its crystallography and chemistry have been described in detail by Hurlbut (1956). This muscovite crystal has a $2M_1$ structure, with an optic axial angle ($2V$) of 45°38′ as determined from its refractive indices. Its composition, $K_{1.75}\,Na_{0.27}\,Ca_{0.00}\,(Al_{3.82}\,Fe_{0.27}\,Mg_{0.01}\,Ti_{0.01})\,(Si_{5.93}\,Al_{2.07})\,O_{20}\,(OH_{0.98}\,F_{0.02}\,Cl_{0.00})_4$, was determined using a Cameca SX-50 electron microprobe, assuming four formula units (OH + F + Cl) and normalizing to oxygen, in good agreement with Hurlbut's formula determined by wet chemical analyses. An independent determination of hydrogen content (4.13 ±

0.09 OH per formula unit) was made by D. Dyar (personal communication) using an H-extraction method described by Holdaway *et al* (1986).

Sample preparation

The orientations of the crystallographic axes *a* and *b* were determined from interference figures using a petrographic microscope. Since coring muscovite in arbitrary orientations is not possible, the crystal was cut into rectangular prismatic samples using a wire saw operating at low cutting loads. The crystal was impregnated with cyanoacrylate ester before cutting to prevent disintegration and minimize damage of samples during preparation. Slabs were first cut perpendicular to the basal plane (001) and parallel to [100], [310], [110] and [010]. From each of these slabs, individual samples were cut, measuring approximately 15 × 6 × 6 mm, with their long dimensions at 0°, 45° and 90° to the basal plane so as to maximize and minimize the shear stress resolved on (001) in the triaxial compression experiments. Stainless steel wires, 0.25 mm in diameter, were used with a slurry consisting of a mixture of silicon carbide (600 grit), glycerine and water. The cutting rate was adjusted to minimize damage to the muscovite. The cyanoacrylate ester was removed from samples after placing them into their jackets, but before sealing them, by heat treatment in a muffle furnace at 400°C for 24–36 h, as described in greater detail by Kronenberg *et al.* (1990). Heat treatment at this temperature is not likely to affect the composition of muscovite since dehydroxylation does not occur below 600°C at atmospheric pressure (Vedder & Wilkins 1969). Abundant cleavage-parallel cracks were present in the sample after removal of the cyanoacrylate ester and application of confining pressures high enough to suppress frictional sliding was necessary to investigate dislocation glide for samples compressed at 45° to (001).

Sample assembly and experimental procedure

In order to accommodate the rectangular shape of prismatic samples within the cylindrical shape of the pistons and furnace, samples were placed into silver jackets that were machined to rectangular inner dimensions and cylindrical outer dimensions matching those of the pistons (Fig. 2). All silver components were annealed at 800°C for 24 h prior to sample assembly. Tungsten carbide spacers were used to center the sample in the region of the furnace where the smallest temperature gradient has been measured in temperature calibration tests (~10°C from the sample's center to end). Temperatures during the experiments were measured (at one end of the sample assembly) using a sheathed Chromel–Alumel Thermocouple within a vented piston. A disc of quartzite that had been thermally cracked by prior heat treatment was placed between the sample and the vented piston to prevent extrusion of the sample while ensuring communication of any fluids generated at temperature with the atmosphere. A thin (0.05 mm) silver disc was placed between the sample and the tungsten carbide spacer at one end of the sample to reduce frictional end effects but no silver shim was used between the sample and the quartzite disc. These experiments are considered drained and the applied confining pressures measured should represent true effective pressures. For comparison, several undrained tests were conducted as well, using a solid tungsten carbide spacer in place of the quartzite disc that would not allow fluids to escape.

Some samples were deformed at several conditions in temperature- and strain rate-stepping tests in order to determine the effects of temperature and strain rate, respectively, on basal shear strength without introducing scatter in the data resulting from sample-to-sample variations. Temperature-stepping tests were performed, in which the same sample was step-wise deformed at several temperatures while maintaining a constant confining pressure and imposing the same strain rate, beginning deformation at 400°C and ending at 30°C. This sequence was chosen to minimize work hardening of the silver jackets early in the test which might lead to errors in jacket strength corrections. Each experimental step was carried out until it was evident that the differential stress supported by the sample was relatively constant with increasing strain. The sample was unloaded after each experimental step before decreasing the temperature for the next increment. Unloading was necessary since temperature changes cause length changes in the force gauge used to measure axial loads. A new reading, corresponding to zero differential stress, was measured at each temperature once thermal equilibrium had been established. The effect of strain rate on the strength of muscovite was investigated by measuring differential stresses at a temperature of 400°C and a confining pressure of 200 MPa for several strain rates, beginning with 10^{-4} s^{-1} and step-wise reducing the rate to 10^{-5}, 10^{-6} and 10^{-7} s^{-1}. As in temperature-stepping experiments, samples were unloaded between each step. Each step was carried out until the differential stress supported by the sample was relatively constant with increasing strain.

All samples were deformed using a Heard-type triaxial gas apparatus (Heard & Carter 1968) with argon as the confining medium. An internal platinum wire furnace generated the desired experimental temperatures. Muscovite samples were shortened at confining pressures P_c from 11 to 400 MPa, temperatures T from 20 to 400°C, and strain rates $\dot{\varepsilon}$ from 2.5×10^{-7} to 2.3×10^{-4} s^{-1}. The pressures and temperatures during experiments were servo-controlled to ±2 MPa and ±1°C, respectively. Approximately constant strain rates were achieved by the use of a synchronous motor and gear train engaged to a ball-bearing screw and thrust bearing. Corrections to differential stress supported by samples due to the strengths of the silver jackets were large (relative to the low strength of muscovite) and several experiments were performed to determine the strengths of the silver jackets at the conditions of the experiments. Silver jacket strengths were determined by shortening

cleaved single crystal halite samples in silver jackets of the same dimensions as those used for the muscovite experiments, at the same conditions and using the same procedures as those used for muscovite experiments. For temperature- and strain rate-stepping experiments jacket strength calibrations were determined using the same temperature and strain rate paths, respectively, on jacketed halite samples as were used in the muscovite experiments and imposing the same incremental strains for each step. The reproducibility of strength determinations for the machined silver jackets, based upon repeat calibration tests, is approximately ±3 MPa. However, larger variations in strength were encountered for muscovite samples due to imperfections in their geometry. Silver jacket calibration data are listed in the appendix, deducting strengths of halite as reported by Carter & Heard (1970).

Optical and electron microscopy

The deformed samples were impregnated with epoxy resin and cut in half perpendicular to their basal planes using a low-speed diamond wafering saw. Standard thin sections (30 μm thick) were prepared from selected samples to observe the optically resolvable deformation microstructures. Thin (001)-parallel foils (<1 μm thick) were prepared for TEM by cleavage and ion milling, and dislocations were imaged in bright field using a JEOL 2010 under two-beam diffraction conditions.

RESULTS

The strengths of muscovite samples deformed with the compression axis oriented at 45°, 0° and 90° to the basal plane at $T = 400$°C, $P_c = 200$ MPa and $\dot{\varepsilon} = 10^{-5}$ s^{-1} vary by approximately a factor of 50 (Fig. 3). Low strengths were measured for samples loaded at 45° to (001) with homogeneous shear (Fig. 4a) accommodated by dislocation glide. Samples compressed at 0° to (001) showed intermediate strengths with deformation accommodated by the formation of kink bands (Fig. 5). The highest strengths were measured for samples compressed at 90° to (001) which failed by fracture (Fig. 4b). Stress–strain curves associated with the relatively homogeneous shear of samples loaded at 45° to (001) exhibit a shallow, linear slope followed by gentle yielding and steady, nearly constant strength thereafter. Stress–strain curves for samples that deformed by kink band development are characterized by an initially steep elastic slope followed by slight inelastic yielding before reaching a sharply defined peak stress and subsequent stress drop. Thereafter the stress–strain curves show relatively steady behavior for the remainder of the experiment with some reduction of strength with increasing strain. Representative stress–strain curves for fracture across cleavage in samples loaded perpendicular to (001) are characterized by a steep linear elastic slope with little evidence of inelastic yielding prior to failure at high differential stresses.

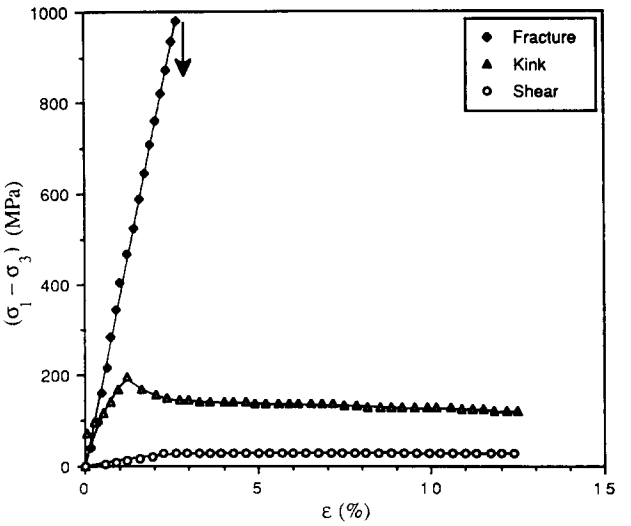

Fig. 3. Stress–strain curves for muscovite samples oriented favorably for shear, kink generation, and fracture at $T = 400$°C, $P_c = 200$ MPa and $\dot{\varepsilon} = 10^{-5}$ s^{-1}. The stress–strain curve for shear on (001) by dislocation glide (compression at 45° to (001) and [010], experiment M-32) is characterized by a shallow linear slope, followed by gentle yielding and by continued deformation at low, approximately constant stress levels for the remainder of the experiment. The stress–strain curve associated with kink generation (compression parallel to (001) and [010], experiment M-46) shows an initial linear elastic slope followed by a peak strength of 194 MPa at 1.2% strain and later strain-softening. Fracture across cleavage (compression perpendicular to (001), experiment M-42) occurs following a linear elastic reponse with little or no yielding prior to a sharply defined peak stress of 982 MPa.

The following sections address the mechanical results and mechanisms of deformation for these three orientations, beginning with samples shortened at 45° to (001) that deformed by dislocation glide, followed by those that deformed by kink generation and finally those that failed by fracture.

Dislocation glide in samples shortened at 45° *to* (001)

Samples compressed at 45° to their basal planes deformed primarily by dislocation glide over a broad range of conditions tested (50 MPa $\leq P_c \leq$ 400 MPa, 20°C $\leq T \leq$ 400°C, 10^{-7} s^{-1} $\leq \dot{\varepsilon} \leq 10^{-4}$ s^{-1}), as evidenced by undulatory extinction (Fig. 4a). With few exceptions kink boundaries in samples of this orientation are absent within sample interiors and appear only at the sample ends as a result of friction between the rigid pistons and the sample and other end effects. The mechanical response associated with deformation in this orientation is summarized in Table 1. Results of temperature-stepping and strain rate-stepping experiments are listed in greater detail in Tables 2 and 3, respectively. Individual test results were used to examine the effects of pressure and shear direction within the basal plane of samples from all four orientations, conducted at the same T, P and $\dot{\varepsilon}$, while stepping experiments were used to determine the relatively small temperature and strain rate effects on glide strength.

Pressure effects. The pressure sensitivity of muscovite samples loaded at 45° to (001) was tested from 11 to 400 MPa at a constant temperature of 400°C and a strain rate

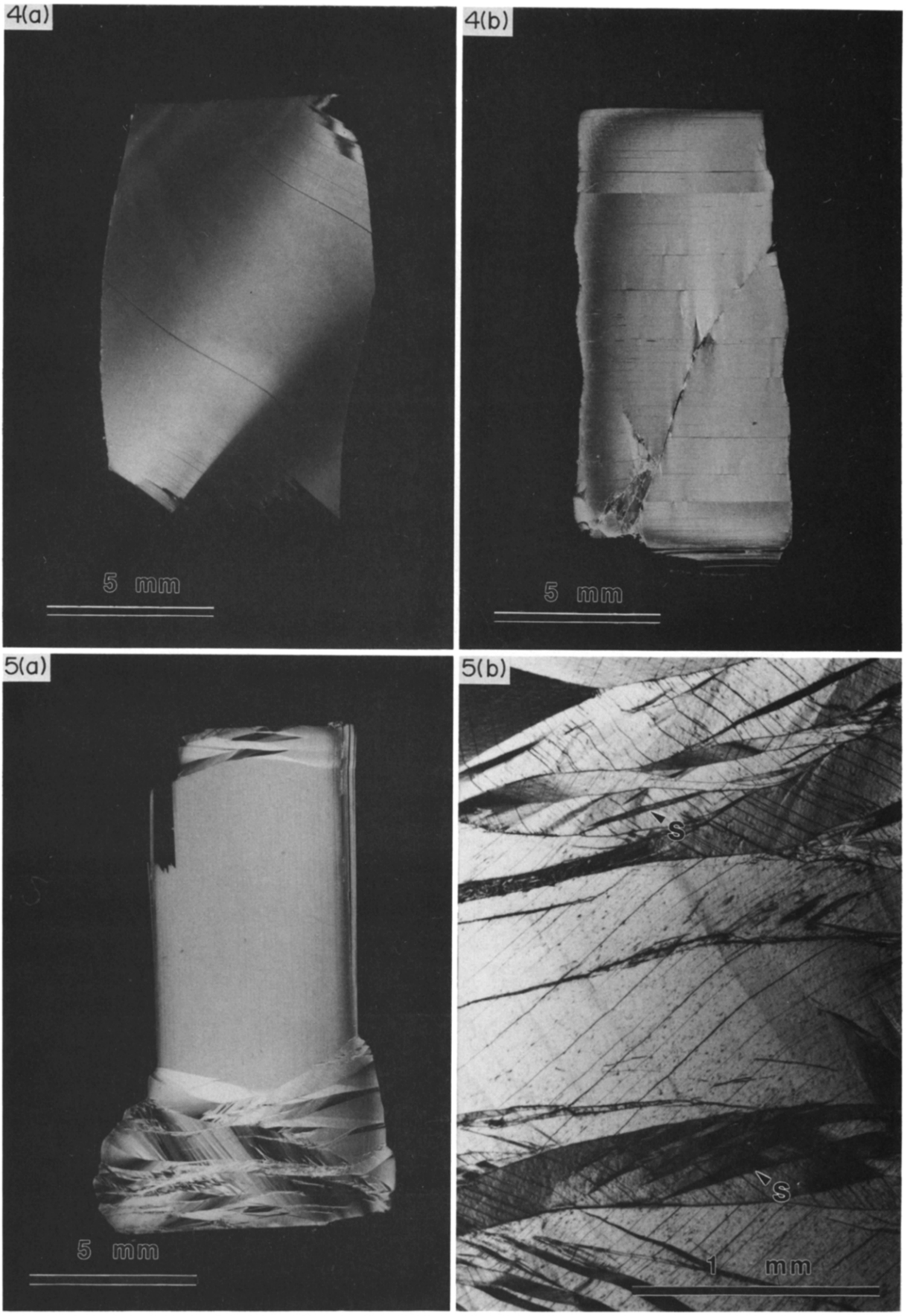

Fig. 4. (a) Whole-sample optical micrograph of muscovite (sample M-11), compressed at 45° to (001) at $T = 400°C$, $P_c = 200$ MPa and $\dot{\varepsilon} = 10^{-5}\ s^{-1}$. (b) Whole sample micrograph of muscovite (sample M-43), compressed perpendicular to (001) at $T = 400°C$, $P_c = 200$ MPa and $\dot{\varepsilon} = 10^{-5}\ s^{-1}$.

Fig. 5. (a) Whole-sample micrograph of muscovite (sample M-48), compressed parallel to (001) at $T = 400°C$, $P_c = 100$ MPa and $\dot{\varepsilon} = 10^{-5}\ s^{-1}$. (b) Detail of kinked end of sample M-48 shown in (a) with fine-scale second (S) and later generation kink bands formed within mm-scale first-generation kink bands.

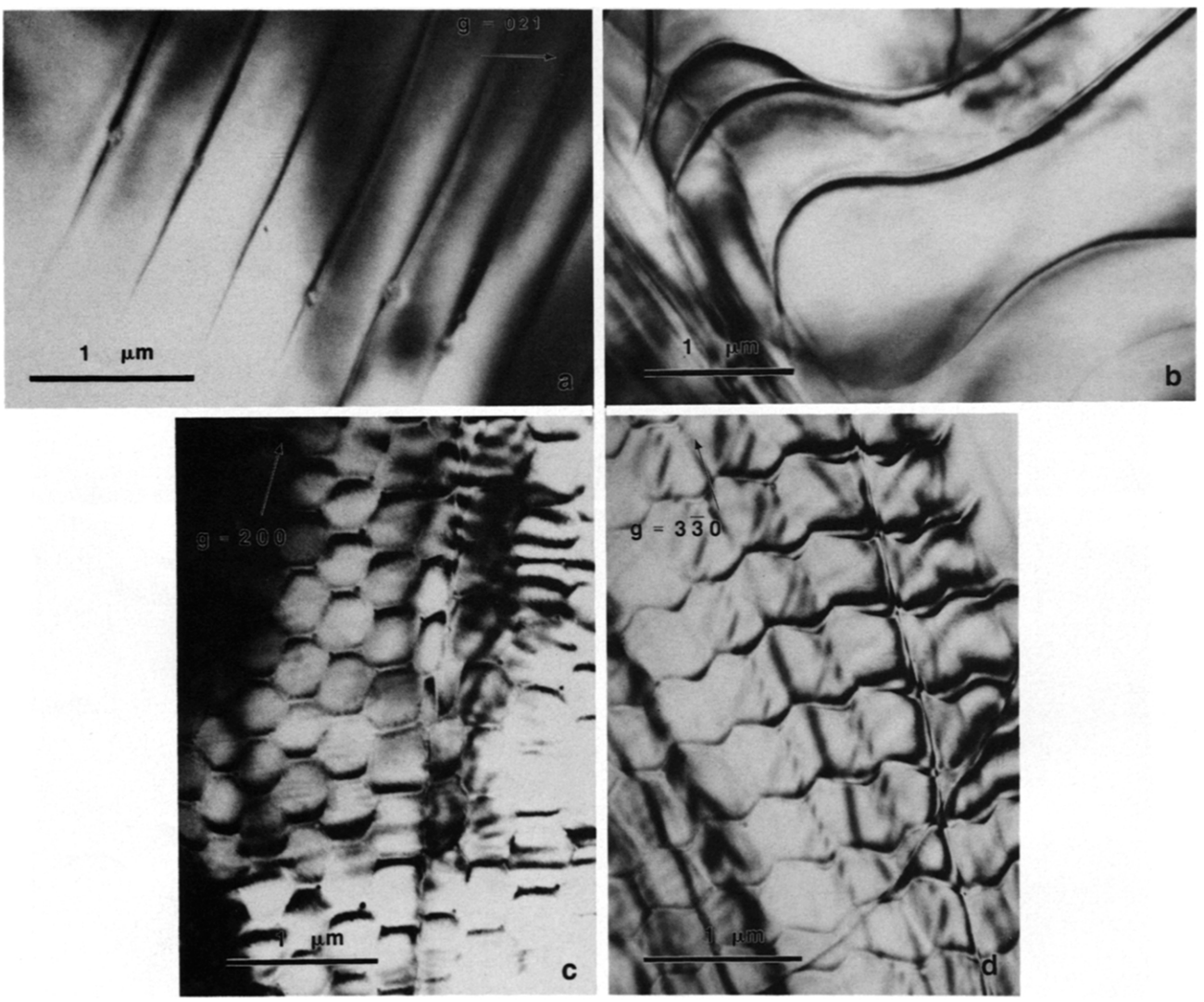

Fig. 9. TEM micrographs of sets of (a) straight and (b) curvilinear dislocations within the (001) plane of deformed muscovite (sample M-11, compressed at 45° to (001) and [310] at $T = 400°C$, $P_c = 200$ MPa and $\dot{\varepsilon} = 10^{-5}\ s^{-1}$). (c) TEM micrograph of dislocation network in the (001) plane of muscovite (sample M-25, compressed at 45° to (001) and [110] at $T = 400°C$, $P_c = 200$ MPa and $\dot{\varepsilon} = 10^{-5}\ s^{-1}$. (d) The same area as shown in (c) but tilted with $g = 3\bar{3}0$. Under these diffraction conditions one of the three sets of dislocations in (c) is extinct and likely to have a Burgers vector of 1/2[110]. All foils prepared parallel to (001).

Table 1. Results for samples loaded at 45° to (001)

Exp. No.	Temperature T (°C)	Confining pressure P_c (MPa)	Strain rate $\dot{\varepsilon}$ (s^{-1})	Differential stress $\sigma_1 - \sigma_3$ (MPa) at ε = 1%	3%	5%	10%	Total strain ε (%)
Direction of shear: [100]								
M-1	400	200	2.2×10^{-5}	11	35	35	35	12
M-10*	400	200	2.2×10^{-5}	23	22	16	—	5*
Direction of shear: [110]								
M-29	400	400	2.3×10^{-5}	5	23	30	36	11
M-28	400	300	2.2×10^{-5}	†	10	15	20	12
M-22	400	200	2.2×10^{-5}	12	16	17	18	11
M-25‡	400	200	2.2×10^{-5}	18	22	22	22	12
M-52*	400	200	2.3×10^{-5}	14	19	20	—	5*
M-54§	400	200	2.3×10^{-4}	60	66	64	—	7§
M-31	200	200	2.2×10^{-5}	37	67	64	60	13
M-26‡	200	200	2.1×10^{-5}	36	75	70	70	12
M-23	20	200	2.2×10^{-5}	23	35	36	48	10
M-27‡	20	200	2.2×10^{-5}	23	30	35	44	11
Direction of shear: [310]								
M-11	400	200	2.3×10^{-5}	16	27	32	34	14
M-18*	400	200	2.2×10^{-5}	34	40	36	—	5*
M-12	400	100	2.2×10^{-5}	17	30	33	37	12
M-14	400	50	2.3×10^{-5}	22	37	40	41	12
M-16	400	25	2.4×10^{-5}	12	24	27	33	13
M-15	400	11	2.4×10^{-5}	†	0.5	5	7	13
Direction of shear: [010]								
M-32	400	200	2.2×10^{-5}	4	21	26	31	12
M-33	400	200	2.3×10^{-5}	11	19	27	29	12
M-41*	400	200	2.2×10^{-5}	38	44	39	—	5*
M-35§	400	200	2.2×10^{-4}	34	37	36	—	7§
M-36§	400	200	2.3×10^{-4}	16	23	42	—	7§

*Data from first increment of temperature-stepping experiments. For results of temperature-stepping tests see Table 3.
†Differential stress not measurable, given uncertainty in jacket strength correction.
‡Experiments were performed undrained.
§Data from first increment of strain rate-stepping experiments. For results of strain rate-stepping tests see Table 4.

Table 2. Temperature-stepping experiments

Exp. No.	T (°C)	P_c (MPa)	$\dot{\varepsilon}$ (s^{-1})	$\sigma_1 - \sigma_3$ (MPa) at 5% incremental strain	Total cumulative strain (%)	Q/α (kJ-MPa mol^{-1})
Direction of shear: [100]						
M-10	400	200	2.2×10^{-5}	16	5	102
	200		2.3×10^{-5}	16	10	
	100		2.4×10^{-5}	30	15	
	30		2.6×10^{-5}	36	21	
Direction of shear: [110]						
M-52	400	200	2.3×10^{-5}	20	5	109
	200		2.4×10^{-5}	30	10	
	100		2.6×10^{-5}	49	16	
	30		2.7×10^{-5}	40	22	
Direction of shear: [310]						
M-18	400	200	2.2×10^{-5}	36	5	86
	200		2.3×10^{-5}	46	10	
	100		2.4×10^{-5}	54	15	
	30		2.6×10^{-5}	54	21	
Direction of shear: [010]						
M-41	400	200	2.2×10^{-5}	39	5	80
	200		2.4×10^{-5}	48	11	
	100		2.5×10^{-5}	58	16	
	30		2.7×10^{-5}	55	22	

of 10^{-5} s^{-1} in order to determine the conditions over which frictional sliding and dislocation glide are important (Fig. 6). Frictional sliding on (001) is the dominant deformation mechanism for crystals loaded at 45° to cleavage at pressures $P_c < 50$ MPa with a friction coefficient μ of approximately 0.4, in good agreement with that ($\mu \cong 0.36$) determined by Horn & Deere (1962) at room temperature and low normal stress. A change of slope in the Mohr–Coulomb envelope occurs between 50 and 100 MPa and at confining pressures exceeding 100 MPa strength is very nearly independent of normal stress, with an apparent value for the friction coefficient

Table 3. Strain rate-stepping experiments

Exp. No.	T (°C)	P_c (MPa)	$\dot{\varepsilon}$ (s^{-1})	$\sigma_1 - \sigma_3$ (MPa) at $\varepsilon = 2\%$	Total cumulative strain (%)	α (MPa^{-1})
Direction of shear: [110]						
M-54	400	200	2.3×10^{-4}	66	7	0.43
			2.4×10^{-5}	67	10	
			2.5×10^{-6}	55	12	
			2.6×10^{-7}	52*	14	
Direction of shear: [010]						
M-35	400	200	2.2×10^{-4}	35	7	0.79
			2.4×10^{-5}	50	10	
			2.4×10^{-6}	36	12	
			2.5×10^{-7}	30	14	
M-36	400	200	2.3×10^{-4}	20	7	0.29
			2.5×10^{-5}	41	11	
			2.6×10^{-6}	36	13	
			2.6×10^{-7}	25	15	

*Peak stress, measured at 0.5% incremental strain.

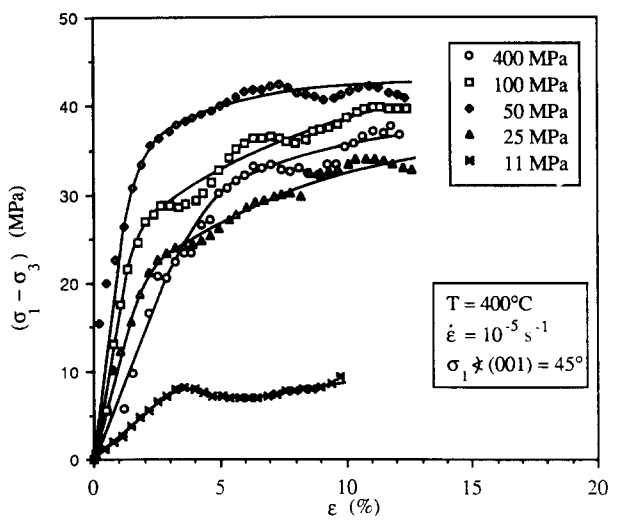

Fig. 6. Stress–strain curves for muscovite samples shortened at 45° to (001) at confining pressures from 11 to 400 MPa (M-29, M-12, M-14, M-16 and M-15). Strengths are strongly dependent upon confining pressure at $P_c < 50$ MPa, whereas strengths of samples deformed at confining pressures of 100–400 MPa are comparable. Fluctuations in the stress–strain curves of ~2–3 MPa are artifacts associated with pressure fluctuations of 2–3 MPa.

μ of 0 (Fig. 7a). Samples deformed at $P_c \leq 50$ MPa exhibit multiple offsets along cleavage but show undulatory extinction as well. Little evidence can be found for frictional sliding in samples deformed at $P_c > 50$ MPa, and microstructures evident in thin section (Fig. 4a) are dominated by smoothly undulatory extinction and external rotations.

Effects of shear direction. The results of experiments performed on samples compressed at 45° to (001) at high confining pressure ($P_c \geq 100$ MPa) suggest a weak mechanical anisotropy within the (001) plane (Fig. 8) similar to that observed for glide in biotite (Kronenberg *et al.* 1990). Although sample-to-sample variations in strength are sizeable for any one shear direction, samples loaded at 45° to the [100] and [110] directions appear to be somewhat weaker (22 ± 8 MPa) than those loaded at 45° to [310] and [010] (32 ± 5 MPa); the weak directions correspond to the Burgers vectors ⟨100⟩, 1/2⟨110⟩, and 1/2⟨$\bar{1}$10⟩ determined previously by Silk & Barnes (1961), Demny (1963) and Meike (1989) on the basis of TEM diffraction contrast and extinction criteria. TEM of samples (M-11, M-23 and M-25) shortened at 45° to (001) and the directions [110] and [310] reveals curvilinear sets of dislocations and dislocation networks that are confined to (001) planes (Fig. 9), leaving foils only at cleavage steps. Consistent with the smooth, undulatory extinction observed optically under crossed polars, dislocations appear evenly distributed throughout the foils examined. Burgers vectors **b** of dislocations identified in these samples include ⟨100⟩ and 1/2⟨110⟩. Any differences in strength between the weak directions [100] and [110] associated with the dioctahedral nature and the distorted tetrahedral sheets of muscovite cannot be detected given the sample-to-sample scatter.

Temperature and strain rate effects. The effects of temperature and strain rate on the basal glide strength of muscovite were investigated at a confining pressure of 200 MPa, sufficient to inhibit frictional sliding. Variations in glide strength associated with sample-to-sample variations are large, however, and temperature- and strain rate-stepping experiments were therefore performed on individual samples to eliminate this source of scatter. The results of stepping tests were evaluated assuming that dislocation glide on (001) can be described by an exponential flow law of the form

$$\dot{\varepsilon} = A \exp(\alpha\sigma) \exp(-Q/RT), \quad (1)$$

where σ is the differential stress $\sigma_1 - \sigma_3$, T is the temperature in kelvins, A and α are material parameters, Q is the activation energy for glide, and R is the gas constant (Poirier 1985). Results from the temperature-stepping experiments, plotting the differential stress $\sigma_1 - \sigma_3$ at 5% strain vs $1/T$, define lines for each of the four directions [100], [110], [310] and [010] with slopes of $Q/\alpha R$. Results from the strain rate stepping experiments, plotting $\sigma_1 - \sigma_3$ vs ln $\dot{\varepsilon}$, define lines with slopes of $1/\alpha$.

Results of temperature-stepping experiments (as-

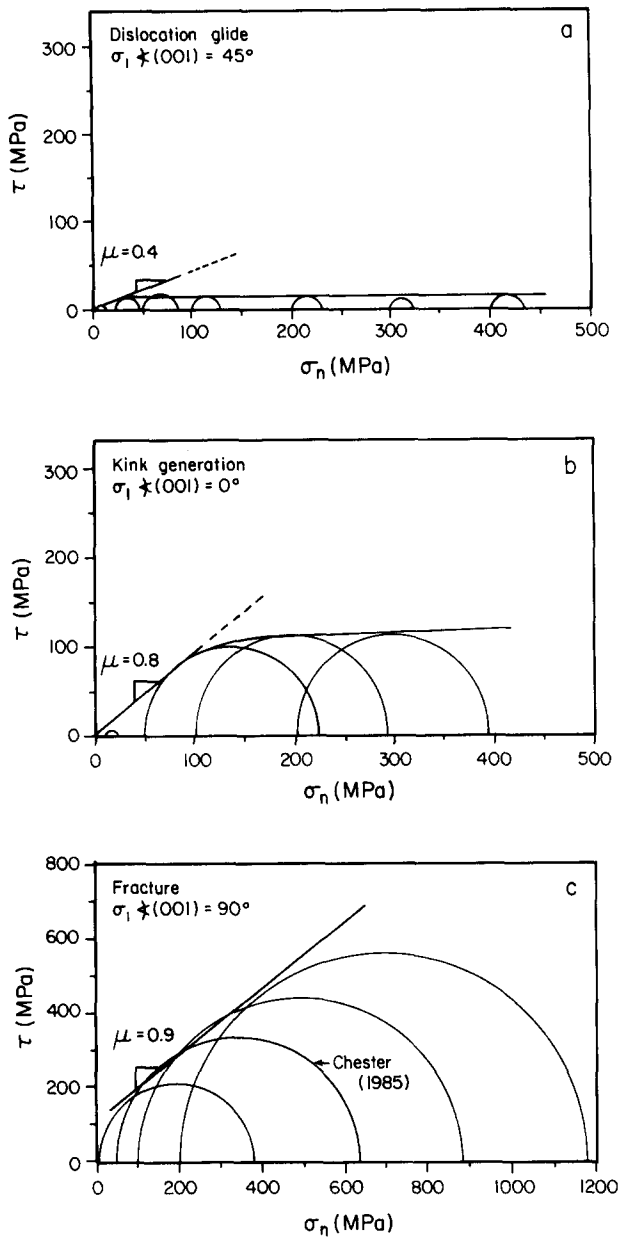

Fig. 7. Mohr–Coulomb envelopes for dislocation glide, kink generation and fracture. (a) Muscovite samples shortened at 45° to (001) at pressures of 11–400 MPa exhibit a slope (or apparent coefficient of friction μ) of ~0.4 for $P_c < 50$ MPa while strengths are nearly independent of pressure and $\mu = 0$ at $P_c > 100$ MPa (samples M-15, M-16, M-14, M-12, M-25, M-28 and M-29). (b) Muscovite samples shortened parallel to (001) deform by kink band development with an apparent coefficient of internal friction of $\mu \cong 0.8$ for samples deformed at $P_c < 100$ MPa and $\mu < 0.1$ for samples deformed at $P_c > 100$ MPa (samples M-60, M-49, M-48 and M-46). (c) Muscovite samples shortened perpendicular to (001) fail by fracture across cleavage at all confining pressures tested ($10 \leq P_c \leq 200$ MPa) and define a slope of $\mu \cong 0.9$ (samples M-44, M-43 and M-42). The experiment shown at $P_c = 50$ MPa with a peak strength of 575 MPa is taken from Chester (1985).

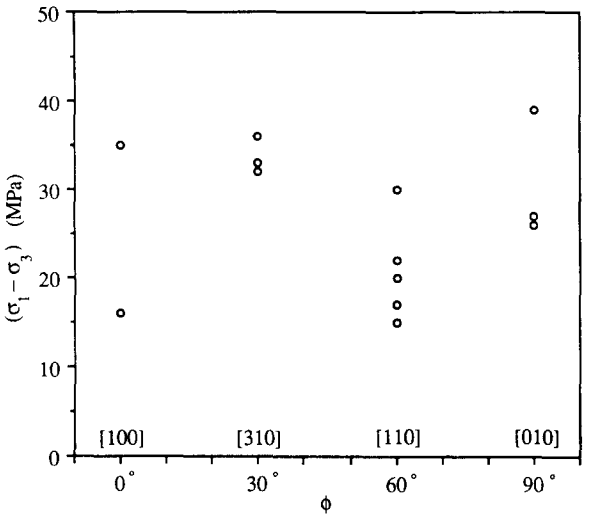

Fig. 8. Plot of strength vs shear direction within (001) for muscovite samples compressed at 45° to (001). The angle ϕ is measured within the basal plane from the a-axis. Differential stresses measured at $\varepsilon = 5\%$ for samples compressed at 45° to (001) and to the directions [100], [310], [110] and [010] at $T = 400$°C, $P_c \geq 100$ MPa and $\dot{\varepsilon} = 10^{-5}$ s^{-1} suggest a weak anisotropy within the basal plane with minimum shear strengths in directions [100] and [110]. This weak anisotropy is consistent with the slip systems reported by Silk & Barnes (1961), Demny (1963) and Meike (1989) and resembles the anistropy observed for biotite (Kronenberg *et al.* 1990). The experimental data plotted include those for experiments M-1, M-10, M-11, M-12, M-18, M-22, M-25, M-28, M-29, M-52, M-32, M-33 and M-41.

sembled in Table 2) reveal small but systematic increases in strength with stepwise reductions in temperature at constant confining pressure and strain rate (Figs. 10a & b). The temperature dependence of glide strength appears to be the same in all four orientations tested (Fig. 10c), even though strengths measured for the different shear directions in (001) suggest some anisotropy. The average value of Q/α (using the results of M-10, M-52, M-18 and M-41) is 94(±12) kJ-MPa mol^{-1}.

Strain rate-stepping experiments reveal only small changes in strength with large changes in strain rate (Table 3). As a result, values of $1/\alpha$ given by the slopes of these data, plotting $\sigma_1 - \sigma_3$ vs ln $\dot{\varepsilon}$, are difficult to determine and show considerable scatter (Fig. 11). However, taking the mean of slopes determined for both the [110] and [010] orientations, a value for α of approximately 0.5 ± 0.2 MPa^{-1} may be estimated. Using the combined results of these stepping experiments to determine Q and α, and using all of the strength measurements for samples compressed at 45° to (001) at $P_c \geq 100$ MPa to determine values for the pre-exponential constant A, deformation of muscovite by (001) glide may be described by equation (1) where:

$$Q = 47 \pm 19 \text{ kJ mol}^{-1}$$

$$\alpha = 0.5 \pm 0.2 \text{ MPa}^{-1}$$

$$A \cong 1 \times 10^{-6} \text{ s}^{-1} \text{ for [100] and [110]}$$

$$A \cong 4 \times 10^{-9} \text{ s}^{-1} \text{ for [010] and [310].}$$

In addition to the temperature- and strain rate-stepping experiments designed to determine material parameters, samples of muscovite were loaded at 45° to (001) and [110] at temperatures of 20 and 200°C (Table 1) and compared with samples deformed at 400°C to test for any changes in microstructure. Undulatory extinction revealed by optical microscopy of these samples is indistinguishable from that exhibited by samples deformed at 400°C and TEM shows that similar dislocation arrangements developed in samples deformed at 20°C (M-23) and 400°C (M-25).

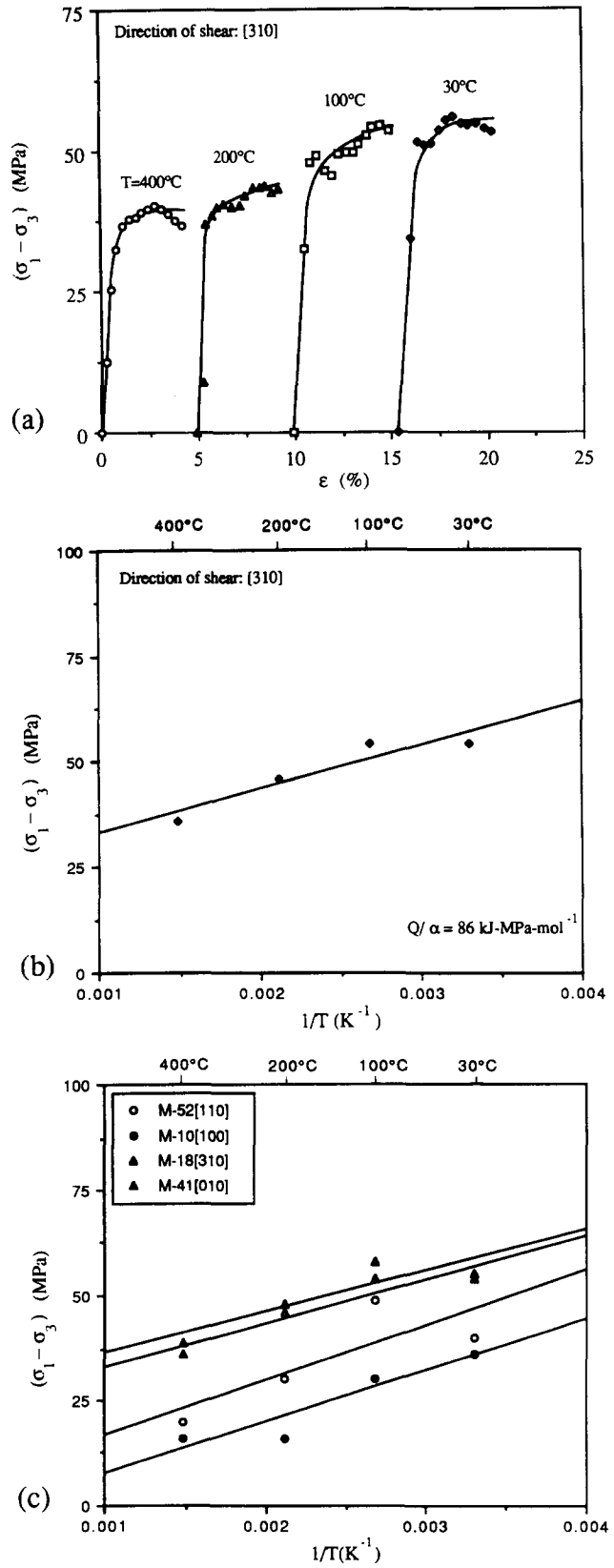

Fig. 10. Results of temperature-stepping experiments for samples loaded at 45° to (001). (a) Stress–strain curves for each of the individual steps of experiment M-18, beginning with $T = 400°C$ and ending with $T = 30°C$. The sample was shortened to approximately 5% strain at each temperature and a mean stress was determined for each temperature from the data following each yield point. (b) Plotting the results of M-18 as differential stress $(\sigma_1 - \sigma_3)$ vs $1/T$, the data define a line with a slope corresponding to $Q/\alpha \cong 86$ kJ-MPa mol^{-1}. (c) Plot of differential stress vs $1/T$ for samples oriented for shear in directions [100], [110], [310] and [010] (experiments M-10, M-52, M-18 and M-41, respectively). Slopes determined from these data yield a mean value of Q/α of 94 ± 12 kJ-MPa mol^{-1}.

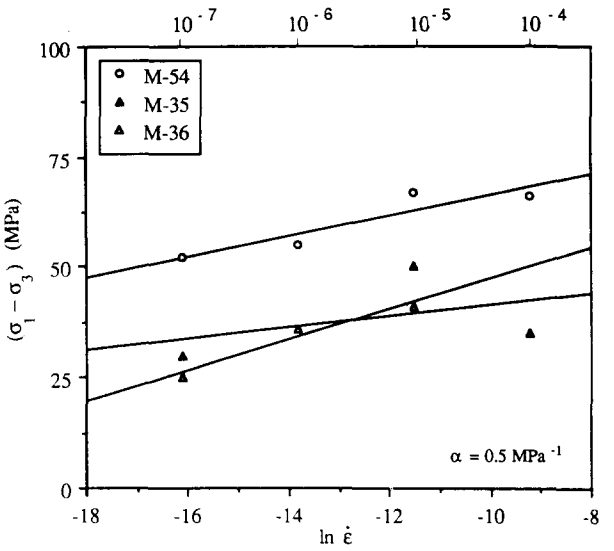

Fig. 11. Differential stress $(\sigma_1 - \sigma_3)$ vs $\ln \dot{\varepsilon}$ for samples compressed at 45° to (001), plotting the data from three strain-rate stepping experiments (M-54, M-35 and M-36). Taking the average over these slopes yields a value for α of ~0.5 MPa^{-1}.

Kink generation in samples shortened at 0° *to* (001)

Compression of muscovite parallel to the basal plane results in the formation of kink bands at high angles to the compression direction (Fig. 5). In all samples kink bands developed in greater numbers at the sample end that was in contact with the quartzite spacer at the vented piston and in fewer numbers near the shorter, stationary piston. Experiments were conducted at confining pressures ranging from 10 to 200 MPa, at a temperature of 400°C, and a strain rate of 10^{-5} s^{-1}. The results of these tests are listed in Table 4. At low confining pressure (10 MPa) a peak differential stress is reached relatively late in the record (at 6.8% strain) followed by a small stress drop of approximately 0.3 MPa. A subsequent stress drop of 2 MPa occurred gradually over approximately 3% strain and no stress drops occurred at higher strains. At 50, 100 and 200 MPa peak differential stresses are reached early in the record (at 1–2.5% strain), followed by stress drops and strain softening from 5 to 30 MPa; however, stresses at large strains (Fig. 3) continue to be larger than strengths measured for samples loaded at 45° to (001). Thereafter, stress–strain records show small, but repeated strain-hardening and strain-softening events with stress drops of 5–10 MPa, presumably associated with kink formation. Peak stresses define a non-linear Mohr–Coulomb envelope (Fig. 7b) with a slope of $\mu \cong 0.8$ for confining pressures below 100 MPa and μ approaching 0 at higher confining pressures.

With increasing confining pressure, the volume fraction of the sample that contains kink bands appears to decrease and closely-spaced kink bands become narrower. Sample M-60, deformed at 10 MPa confining pressure, shows separation along cleavage and bending of separated, cleavage-parallel segments, broadly defining a kink band that traverses the entire width of the sample. In one portion of this sample cleaved segments

Table 4. Results for samples loaded parallel to (001) and [010]

Exp. No.	T (°C)	P_c (MPa)	$\dot{\varepsilon}$ (s^{-1})	Peak differential stress (MPa)	ε at peak differential stress (%)	$\sigma_1 - \sigma_3$ (MPa) at ε = 5%	ε = 10%	Total strain (%)
M-46	400	200	2.2×10^{-5}	194	1.2	138	127	12.5
M-48	400	100	2.1×10^{-5}	189	1.9	172	157	11
M-49	400	50	2.2×10^{-5}	170	2.5	125	120	10
M-60	400	10	2.6×10^{-5}	10	6.8	8	8	14

Table 5. Results for samples loaded perpendicular to (001)

Exp. No.	T (°C)	P_c (MPa)	$\dot{\varepsilon}$ (s^{-1})	Peak differential stress (MPa)	Strain at peak differential stress (%)	Total strain (%)
M-42	400	200	2.3×10^{-5}	982	2.7	4.5
M-43	400	100	2.4×10^{-5}	783	3.1	6.6
M-44	400	10	2.4×10^{-5}	369	3.4	4.9

have bent by angles exceeding 120° and basal segments have fractured across cleavage. Finer scale kink bands, 0.5 mm in width, are present as well; however, deformation at this low confining pressure was influenced by sliding between the sample and the quartzite spacer and sample ends did not remain coaxial. At a confining pressure of 50 MPa, ~30% of the sample (M-49) was intensely kinked with relatively wide (~1.2 mm) kink bands. Sample M-48, deformed at P_c = 100 MPa (Figs. 5a & b), shows a region of kinking that measures about 4.4 mm (or ~30% of the sample). Using criteria proposed by Etheridge *et al.* (1973), several generations of kink bands can be distinguished. First generation kink bands measure approximately 1 mm in width while later generation kink bands commonly form within the wider, early formed kink bands, and are narrower. Many second and later generation kink bands have widths that are below optical resolution. Kink band boundaries curve smoothly and many of the wider kinks traverse the entire width of the sample. Sample M-46, deformed at 200 MPa, contains a narrow zone of kink bands, measuring approximately 3.3 mm in width and comprising ~25% of the sample. Individual kink bands are sinuous and some coalesce while others die out. The first generation kink bands have widths of up to 0.8 mm. Later generation kinks within the wider, earlier formed kink bands, have boundaries at high angles (~50°) to those of preceding generations. Several areas show narrow, late generation kink bands which formed so closely together that they cannot be resolved optically.

Fracture in samples shortened at 90° *to* (001)

Muscovite samples loaded perpendicular to (001) deformed by fracture at stresses far greater than those associated with dislocation glide or with kink generation (Table 5 and Fig. 3). Peak differential stresses are reached with little or no yielding and are strongly dependent on pressure, varying from 369 MPa (measured at 3.4% strain) at P_c = 10 MPa to 982 MPa (measured at 2.7% strain) at P_c = 200 MPa. The Mohr–Coulomb envelope for fracture defines a steep slope of $\mu \cong 0.9$ (Fig. 7c), similar to envelopes associated with brittle fracture of other silicates deformed at the same conditions (Paterson 1978). Sharply defined fractures traverse the entire widths of samples and are oriented at ~25–30° to the compression axis (Fig. 4b). Kink bands with boundaries approximately parallel to the compression axis occur adjacent to the fracture surfaces, presumably to accommodate frictional sliding at fracture irregularities.

DISCUSSION

The mechanical response of muscovite is similar to that of biotite (Kronenberg *et al.* 1990), as may be expected from the similar chemistries and structures of their cation interlayers. Relative to other silicates (Kirby & Kronenberg 1987, Evans & Dresen 1991) both micas are weak when shortened at 45° to (001). Both show similar anisotropy with maximum strengths measured perpendicular to (001) and minimum strengths measured for samples oriented favorably for (001) glide in the directions [100] and [110] (Fig. 8). The value for α determined from strain rate-stepping experiments on muscovite ($\alpha = 0.5 \pm 0.2\ MPa^{-1}$) is remarkably similar to that for biotite ($\alpha = 0.4 \pm 0.1\ MPa^{-1}$, Kronenberg *et al* 1990). However, there are important differences between the results for (001) glide in muscovite and those for glide in biotite that were not anticipated. Muscovite compressed at 45° to (001) is significantly weaker than biotite at the same conditions (by a factor of two at T = 400°C, P_c = 200 MPa, $\dot{\varepsilon} = 10^{-5}\ s^{-1}$), and its activation energy for glide ($Q \cong 47\ kJ\ mol^{-1}$) is approximately half that measured for glide in biotite ($Q \cong 82$ kJ mol^{-1}, Kronenberg *et al.* 1990).

The low values for shear strength and activation energy of muscovite relative to corresponding values for biotite cannot be explained simply from the respective

interlayer bond strengths of muscovite and biotite, their respective elastic moduli for shear on (001) or their lattice parameters. While slip is thought to occur along the weakly bonded interlayer region (Baños *et al.* 1983), calculations of K–O bond energies of muscovite and biotite suggest slightly higher mean bond energies for the interlayers of muscovite (Giese 1984). Microprobe analyses of the two starting materials, furthermore, show that the interlayer of the muscovite used in this study is completely filled, while 7% of the interlayer cation sites of the biotite deformed by Kronenberg *et al.* (1990) appear to be vacant. In contrast to our comparison of the inelastic shear strengths of muscovite and biotite, the effective elastic modulus G_{001} for shear on (001) of muscovite (G_{001} = 28.8 GPa; Alexandrov & Ryzhova 1961, Amelinckx 1979) is somewhat larger than that of biotite (G_{001} = 21.1 GPa) and Burgers vector magnitudes, based on lattice parameters of the two micas (e.g. a = 0.52 and 0.53 nm for muscovite and biotite, respectively; Bailey 1984), are comparable.

The poor correlation of activation energies for glide in muscovite and biotite with their respective interlayer bond energies suggests that the differences between their mechanical behavior depends upon factors other than the disruption and reconstruction of K–O bonds within dislocation cores. Several microstructural observations suggest that dislocations are distributed differently in the experimentally deformed muscovite and biotite samples and that different scales of dislocation interactions may be responsible for their differing mechanical properties. Samples of muscovite deformed at 45° to (001) show smoothly undulatory extinction with very few low-angle kink boundaries (Fig. 4a) and TEM observations indicate that dislocation densities are relatively homogeneous. In contrast, low-angle kink (or tilt) boundaries are abundant in experimentally deformed biotite, distributed throughout the entire sample (figs. 5 and 6 of Kronenberg *et al.* 1990). Neighboring kink boundaries of biotite loaded at 45° to (001) may have the same sense of rotation and thus do not define true kink bands with boundaries of alternating sign but they share microstructural characteristics with the boundaries of well defined kink bands in micas (e.g. Bell & Wilson 1981, Bell *et al.* 1986) and appear to form by similar glide processes. Transmission electron microscopy (TEM) of the deformed biotite samples (Christofferson & Kronenberg 1993) has shown that dislocations are heterogeneously distributed, at the scale of the optically detected low-angle kink boundaries with complex, localized arrays of dipoles, multipoles, tilt walls and dislocation pile-ups. Dislocation glide in biotite is therefore thought to be limited by the spacing of low-angle kink boundaries once they are established.

The smooth undulatory extinction and homogeneous dislocation densities of muscovite samples relative to those of deformed biotite suggest that dislocation interactions do not occur at the same scale. Thus the low strength of muscovite relative to that of biotite may correlate with longer pile-up distances and dislocation interactions that are less pronounced than those detected in biotite. Although a wide variety of chemical and structural differences between muscovite and biotite may be called upon to explain differing scales of dislocation interaction, we tentatively suggest that differences in the stress fields surrounding dislocation cores may result from vacant octahedral sites of muscovite relative to the fully occupied octahedral layers of biotite. Because the bulk elastic properties of muscovite and biotite (including their effective shear moduli G_{001}) are similar, any differences in elastic stress fields surrounding the disrupted K–O bonds of dislocation cores must arise from near-field relaxations that differ from bulk elastic behavior.

Strengths of muscovite samples compressed parallel to (001) are somewhat higher (peak differential stress of 194 MPa at T = 400°C, P_c = 200 MPa, and $\dot{\varepsilon} = 1 \times 10^{-5}$ s^{-1}) than those measured for biotite (peak differential stress of ~110 MPa at T = 400°C, P_c = 300 MPa, and $\dot{\varepsilon} = 10^{-4}$ s^{-1}, Etheridge *et al.* 1973) deformed in the same orientation. However, relatively strong stainless steel jackets were used in the biotite experiments of Etheridge *et al.* (1973) and closer comparison of stresses required for kinking in muscovite and biotite are probably not warranted. Differences in jacket strengths and the resulting confinement of samples appear to have led to differences in the distribution of kink bands. Sharply defined kink bands in muscovite samples loaded parallel to (001) are found only at the ends of samples where they are in contact with the pistons, whereas kink bands in deformed biotite samples of Etheridge *et al.* (1973) are widely distributed throughout samples and are actually less frequent at their ends. These differing kink distributions are probably not related to intrinsic differences in physical properties, however, since a sample of biotite shortened parallel to (001) by H. Heard (unpublished) exhibits large-angle kink bands only at its ends (we do not know what jacketing material was used). Complex, overlapping kink bands in the biotite sample deformed by H.Heard are most pronounced at one end, much as in our muscovite samples, and its measured peak strength (σ = 209 MPa at T = 300°C, P_c = 300 MPa, and $\dot{\varepsilon} = 4 \times 10^{-4}$ s^{-1}) is comparable to those measured for muscovite at $P_c \geq 100$ MPa. However, low-angle kink boundaries are distributed throughout this biotite sample, unlike the interiors of kinked muscovite samples that lack any detectable variations in crystallographic orientation (Fig. 5a).

The localization of kink bands at the ends of muscovite crystals loaded at 0° to their basal planes, particularly the end in contact with the quartzite spacer, raises questions regarding the mechanism of kink band nucleation and suggests that their formation is closely controlled by imposed boundary conditions. By measuring axes of rotation for kink bands in biotite single crystals loaded parallel to (001), Etheridge *et al.* (1973) showed that dislocation slip on the systems {001} ⟨100⟩, 1/2⟨110⟩ and 1/2⟨$\bar{1}$10⟩ is involved in the development of kink bands, despite the fact that shear stresses on (001) are zero for a perfectly oriented sample and an idealized triaxial state of stress. Buckling has commonly been

suspected to occur prior to the nucleation of kink bands (e.g. Borg & Handin 1966, Paterson & Weiss 1966, Hobbs *et al.* 1976, Nicolas & Poirier 1976) so as to bring the weak plane, (001) in the case of micas, into orientations for which the resolved shear stress is non-zero. However, our measurements of peak stresses associated with kink nucleation in muscovite samples loaded at 0° to (001) and [010] are difficult to reconcile with measurements of shear stress required for slip on (001) in the [010] direction and, by Schmid's law, would require elastic rotations of (001) by 5°.

Nucleation of kink bands is more likely to arise from shear stresses applied at the sample ends by the rigid pistons. Depending upon the differing effective Young's moduli and Poisson's ratios of the sample and pistons and the frictional contacts between them, shear stresses at the sample ends may be large, particularly near the specimen corners (Pickett 1944). By symmetry of the stress tensor, shear stresses on (001) near sample–piston contacts may be large as well and lead to dislocation glide with negligible rotations of (001) prior to the formation of kink bands. Given the elastic moduli of muscovite (Alexandrov & Ryzhova 1961) and of the tungsten carbide (GE Carboloy) pistons and spacers, the solution of Pickett (1944) for a sample loaded in compression to 194 MPa (the peak differential stress measured for kinking in our experiments) predicts shear stresses at the sample ends that exceed 16 MPa (required for basal slip) over most of the sample–piston contact area. Perfect contacts between the sample and pistons, as assumed for this solution, cannot be maintained near the sample corners, however, and shear stresses are likely to be limited by frictional sliding, below those predicted at sample extremities. Nevertheless, shear stresses (limited by friction assuming a friction coefficient μ of ~0.3) are still expected to be large at the ends of samples, where intense kinking is observed. The observation that kink bands developed preferentially in the end of specimens in contact with the quartzite spacer suggests that frictional contact at this end was better and shear stresses were larger than the opposite specimen end in contact with the silver shim and tungsten carbide spacer. Given that the differential stresses required for kinking depend on frictional boundary conditions and the basal shear strengths of muscovite, the curvature of the Mohr envelope defined by peak stresses associated with kink nucleation in samples loaded parallel to (001) (Fig. 7b) may be closely related to the curvature expressed by samples shortened at 45° to (001) that deformed by sliding on cleavage at low pressures ($P_c < 50$ MPa) and glide at high pressures (Fig. 7a).

The fracture strengths of muscovite samples loaded perpendicular to (001) are much larger than strengths measured for the other orientations with steep linear Mohr–Coulomb envelopes and a coefficient of internal friction of ~0.9, similar to those of a wide range of fine-grained igneous and high-grade metamorphic rocks (Paterson 1978). In this orientation, muscovite appears to be much stronger than biotite which exhibits an internal friction coefficient associated with fracture of only ~0.3 (Kronenberg *et al.* 1990). Muscovite grains within polycrystalline rocks may therefore be extremely weak if significant shear stresses are resolved on their basal planes while other muscovite grains may have strengths comparable to the rest of the aggregate.

Finally, we are confident in our comparisons of the mechanical properties of muscovite and biotite because essentially identical experimental methods (with the exception of kinking experiments) were used. However, observations of microstructures in naturally deformed coexisting muscovite and biotite led Wilson & Bell (1979) to suggest that muscovite is stronger in shear than biotite. The observations they report appear to be consistent with their conclusions and we do not know why they differ from the experimental comparisons of strength. The activation energy for glide in muscovite is smaller than that for biotite and the difference in basal shear strength of these micas must therefore change with temperature. However, an inversion in the relative strengths of these micas with changing temperature and strain rate (over ranges appropriate to continental crust) would require changes in the rate-controlling mechanism of deformation.

The very low shear strength of muscovite may have important implications for the deformation of foliated mica-rich rocks of the middle and lower crust. Experimental studies of schist (Shea & Kronenberg 1992, 1993) and gneiss containing biotite (Gottschalk *et al.* 1990) have shown that their strengths and anisotropies are strongly affected by the orientations and distributions of biotite grains. Given the low basal shear strength of muscovite, its presence may likewise reduce the strength of muscovite-bearing rocks and introduce significant anistropy in mechanical behavior.

CONCLUSIONS

Based on experiments performed on muscovite single crystals oriented for compression at 45°, 0° and 90° to the basal plane the following conclusions may be drawn.

(1) Muscovite compressed at 45° to (001) is weak at all conditions tested. Basal shear strengths measured at confining pressures of up to 25 MPa are characterized by a Mohr–Coulomb envelope with a slope of $\mu \cong 0.4$. Basal shear strengths are insensitive to confining pressures over the range $50 \leq P_c \leq 400$ MPa with $\mu \cong 0$. Shear strengths measured at high confining pressures ($P_c > 100$ MPa) depend upon temperature and strain rate. An exponential flow law of the form $\dot{\varepsilon} = A \exp(\alpha\sigma) \exp(-Q/RT)$ can be used to express these effects with an activation energy for dislocation glide, Q, of 47 ± 19 kJ mol^{-1}, and a value for α of 0.5 ± 0.2 MPa^{-1}.

(2) Samples oriented favorably for dislocation glide in the [100] and [110] directions appear to be somewhat weaker than those oriented for shear in the [010] and [310] directions, consistent with the slip systems reported for muscovite (Silk & Barnes 1961). Two pre-exponential constants A have been estimated, one for compression at 45° to [100] and [110] ($A \cong 1 \times 10^{-6}$ s^{-1})

and one for compression at 45° to [310] and [010] ($A \cong 4 \times 10^{-9}\ s^{-1}$) that describe the anisotropy within the (001) plane. However, these parameters are poorly constrained due to sample-to-sample variations and are not known to better than several orders of magnitude.

(3) Strengths of samples compressed parallel to (001), that deformed by the development of sharply defined kink bands, exceed those of samples compressed at 45° to (001). Peak stresses measured in this orientation define a nonlinear Mohr–Coulomb envelope with $\mu \cong 0.8$ at $P_c < 100$ MPa while $\mu < 0.1$ at $P_c \cong 200$ MPa. Strain softening is observed following the peak in stress, but measured stresses remain higher than those determined for samples compressed at 45° to (001) at strains up to 12%. The initiation of kink bands in these experiments does not appear to involve elastic flexure, as is commonly supposed. Instead, nucleation appears to occur by dislocation glide on (001) in response to shear stresses applied at the ends of samples.

(4) Samples compressed perpendicular to (001) deform by fracture. They exhibit strengths far greater than those of samples loaded in other directions and are strongly dependent upon pressure with $\mu \cong 0.9$, similar to values of internal friction coefficients reported for brittle failure in other silicates.

(5) Comparisons of the data for muscovite with data obtained for biotite single crystals (Etheridge *et al.* 1973, Kronenberg *et al.* 1990) indicate that the basal glide strengths of muscovite (measured for samples compressed at 45° to (001)) in all crystallographic directions within (001) are ~50% lower than those of biotite deformed at the same experimental conditions. Muscovite samples shortened parallel to (001) exhibit peak stresses similar to (or perhaps slightly higher than) those measured for biotite. Muscovite crystals shortened perpendicular to (001) are significantly stronger than biotite deformed at the same confining pressures.

(6) Comparison of optical-scale undulatory extinction and dislocation distributions of muscovite and biotite samples shortened at 45° to (001) suggests that differences in their basal shear strengths may be associated with differing scales of dislocation interaction that correlate with the establishment of low-angle kink boundaries and barriers to dislocation glide. Muscovite samples loaded at 45° to (001) exhibit smooth undulatory extinction and finely spaced, low-angle kink boundaries are rare by comparison with experimentally deformed biotite samples.

Acknowledgements—This work was supported by NSF grant EAR-8816283. The Department of Geology provided additional financial assistance to V. Mares. We thank D. Dyar for the hydrogen analysis and R. N. Guillemette for the high-quality microprobe analyses of the muscovite starting material. Advice and helpful comments by J. Logan, N. Carter and M. Darensbourg, and reviews by Q. Bai and W. Durham are gratefully acknowledged. We thank J. Magouirk for laboratory support, R. McNeely for office support, and the TAMU Electron Microscopy Center for assistance with the TEM.

REFERENCES

Alexandrov, K. S. & Ryzhova, T. V. 1961. Elastic properties of rock-forming minerals. II. Layered silicates. *Bull. (Izv.) Acad. Sci. USSR., Geophys. Ser.* **12**, 1165–1168.

Amelinckx, S. 1979. Dislocations in particular structures. In: *Dislocations in Solids, Volume* 2 (edited by Nabarro, F. R. N.). North-Holland, Amsterdam, 67–460.

Appelo, C. A. J. 1979. Layer deformation and crystal energy of micas and related minerals. II. Deformation of the coordination units. *Am. Miner.* **64**, 424–431.

Bailey, S. W. 1984. Micas. *Rev. Mineral.* **13**, 584.

Baños, J. O., Amouric, M., de Fouquet, C. & Baronnet, A. 1983. Interlayering and interlayer slip in biotite as seen by HRTEM. *Am. Miner.* **68**, 754–758.

Bell, I. A. & Wilson, C. J. L. 1981. Deformation of biotite and muscovite: TEM microstructure and deformation model. *Tectonophysics* **78**, 201–228.

Bell, I. A., Wilson, C. J. L., McLaren, A. C. & Etheridge, M. A. 1986. Kinks in mica: role of dislocations and (001) cleavage. *Tectonophysics* **127**, 49–65.

Borg, I. Y. & Handin, J. W. 1966. Experimental deformation of crystalline rocks. *Tectonophysics* **3**, 249–368.

Borg, I. Y. & Heard, H. C. 1970. Experimental deformation of plagioclases. In: *Experimental and Natural Rock Deformation* (edited by Paulitsch, P.). Springer, Berlin, 375–403.

Carter, N. L., Griggs, D. T. & Christie, J. M. 1964. Experimental deformation and recrystallization of quartz. *J. Geol.* **72**, 687–733.

Carter, N. L. & Heard, H. C. 1970. Temperature and rate dependent deformation of halite. *Am. J. Sci.* **269**, 193–249.

Chester, J. S. 1985. Deformation of layered rocks in the ramp regions of thrust faults: a study with rock models. Unpublished M.S. thesis, Texas A&M University, College Station, Texas.

Christie, J. M., Griggs, D. T. & Carter, N. L. 1964. Experimental evidence of basal slip in quartz. *J. Geol.* **72**, 736–756.

Christoffersen, R. G. & Kronenberg, A. K. 1993. Dislocation interactions in experimentally deformed biotite. *J. Struct. Geol.* **15**, 1077–1095.

Demny, J. 1963. Elektronenmikroskopische Untersuchungen an sehr dünnen Glimmerfolien, I & II. *Zt. Naturforsch. A* **18A**, 1088–1101.

Donath, F. A. 1961. Experimental study of shear failure in anisotropic rocks. *Bull. geol. Soc. Am.* **72**, 985–990.

Donath, F. A. 1964. Strength variation and deformational behavior in anisotropic rocks. In: *State of Stress in the Earth's Crust* (edited by Judd, W. R.). Elsevier, New York, 281–298.

Donath, F. A. 1968. The development of kink bands in brittle anisotropic rock. In: *Igneous and Metamorphic Geology* (edited by Larsen, L., Prinz, M. & Manson, V.). *Mem. geol. Soc. Am.* **115**, 453–493.

Etheridge, M. A., Hobbs, B. E. & Paterson, M. S. 1973. Experimental deformation of single crystals of biotite. *Contr. Miner. Petrol.* **38**, 21–36.

Evans, B. & Dresen, G. 1991. Deformation of earth materials: six easy pieces. *Rev. Geophys.* **29**, 823–843.

Giese, R. F. Jr. 1984. Electrostatic energy models of micas. In: *Micas* (edited by Bailey, S. W.). *Rev. Mineral.* **13**, 105–144.

Gottschalk, R. R., Kronenberg, A. K., Russell, J. E. & Handin, J. W. 1990. Mechanical anisotropy of gneiss: failure criterion and textural sources of directional behavior. *J. geophys. Res.* **95**, 21,613–21,634.

Heard, H. C. & Carter, N. L. 1968. Experimentally induced "natural" intragranular flow in quartz and quartzite. *Am. J. Sci.* **266**, 1–42.

Hobbs, B. E., Means, W. D. & Williams, P. F. 1976. *An Outline of Structural Geology*. J. Wiley & Sons, New York.

Holdaway, M. J., Dutrow, B. L., Borthwick, J., Shore, P., Harmon, R. S. & Hinton, R. W. 1986. H content of staurolite as determined by H extraction line and ion microprobe. *Am Miner.* **71**, 1135–1141.

Horn, H. M. & Deere, D. U. 1962. Frictional characteristics of minerals. *Geotechnique* **12**, 319–335.

Hurlbut, C. S. Jr. 1956. Muscovite from Methuen Township, Ontario. *Am. Miner.* **41**, 892–898.

Kirby, S. H. & Kronenberg, A. K. 1987. Rheology of the lithosphere: selected topics. *Rev. Geophys. & Space Phys.* **25**, 1219–1244.

Koch, P. S., Christie, J. M., Ord, A. & George, R. P. Jr. 1989. The effect of water on the rheology of experimentally deformed quartz. *J. geophys. Res.* **94**, 13,975–13,996.

Kronenberg, A. K., Kirby, S. H. & Pinkston, J. C. 1990. Basal slip and mechanical anisotropy of biotite. *J. geophys. Res.* **95**, 19,257–19,278.

Marshall, D. B. & McLaren, A. C. 1977. Deformation mechanisms in experimentally deformed plagioclase feldspars. *Phys. Chem. Miner.* **1**, 351–370.

Meike, A. 1989. In situ deformation of micas: a high-voltage electron-microscope study. *Am. Miner.* **74**, 780–796.

Nicolas, A. & Poirier, J. P. 1976. *Crystalline Plasticity and Solid State Flow in Metamorphic Rocks*. J. Wiley & Sons, New York.
Paterson, M. S. 1978. *Experimental Rock Deformation—The Brittle Field*. Springer, New York.
Paterson, M. S. & Weiss, L. E. 1962. Experimental folding in rocks. *Nature* **195**, 1045–1046.
Paterson, M. S. & Weiss, L. E. 1966. Experimental deformation and folding in phyllite. *Bull. geol. Soc. Am.* **77**, 343–374.
Pickett, G. 1944. Application of the Fourier method to the solution of certain boundary problems in the theory of elasticity. *J. appl. Mech.* **11**, A176–A182.
Poirier, J-P. 1985. *Creep of Crystals*. Cambridge University Press, New York.
Radoslovich, E. W. 1960. The structure of muscovite, $KAl_2(Si_3Al)O_{10}(OH)_2$. *Acta cryst.* **13**, 919–932.
Shea, W. T. & Kronenberg, A. K. 1992. Rheology and deformation mechanisms of an isotropic mica schist. *J. geophys. Res.* **97**, 15,201–15,237.
Shea, W. T. & Kronenberg, A. K. 1993. Strength and anisotropy of foliated rocks with varied mica contents. *J. Struct. Geol.* **15**, 1097–1121.
Silk, E. C. H. & Barnes, R. H. 1961. The observation of dislocations in mica. *Acta metall.* **9**, 558–562.
Tullis, J. 1983. Deformation of feldspars. *Rev. Miner.* **2**, 297–323.
Tullis, J. & Tullis, T. E. 1972. Preferred orientation of quartz produced by mechanical Dauphine twinning: thermodynamics and axial experiments. In: *Flow and Fracture of Rocks* (edited by Heard, H. C., Borg, I. Y., Carter, N. L. & Raleigh, C. B.). *Am. Geophys. Un. Geophys. Monogr.* **16**, 67–82.
Vedder, W. & Wilkins, R. W. T. 1969. Dehydroxylation and rehydroxylation, oxidation and reduction of micas. *Am. Miner.* **54**, 482–509.
Willaime, C., Christie, J. M. & Kovacs, M.-P. 1979. Experimental deformation of K-feldspar single crystals. *Bull. Miner.* **102**, 168–177.
Wilson, C. J. L. & Bell, I. A. 1979. Deformation of biotite and muscovite: Optical microstructure. *Tectonophysics* **58**, 179–200.

APPENDIX

Table A1. Silver jacket strengths

Exp. No.	T (°C)	P_c (MPa)	$\dot{\varepsilon}$ (s^{-1})	$\sigma_1 - \sigma_3$ (MPa) at ε = 1%	3%	5%	10%	Total ε (%)
Constant strain rate tests								
Na-5	600	200	2.6×10^{-5}	11	12	12	14	15
Na-1	400	200	2.2×10^{-5}	15	15	15	13	15
Na-4	400	200	1.9×10^{-5}	20	21	18	16	15
Na-3	200	200	2.1×10^{-5}	39	48	59	66	15
Na-2	25	200	2.1×10^{-5}	69	93	104	115	15
Temperature-stepping tests								
Na-6	400	200	2.2×10^{-5}	21	25	30	—	5
	200	200	2.3×10^{-5}	42	54	63	—	5
	100	200	2.5×10^{-5}	78	89	92	—	6
	30	200	2.6×10^{-5}	110	112	116	—	6
Strain rate-stepping tests								
Na-11	400	200	2.2×10^{-4}	25	33	37	—	7
	400	200	2.3×10^{-5}	16	19	—	—	4
	400	200	2.4×10^{-6}	9	17	—	—	3
	400	200	2.5×10^{-7}	13	13	—	—	3